CARBON 60 (2013) 157–168

Available at www.sciencedirect.com

SciVerse ScienceDirect

journal homepage: www.elsevier.com/locate/carbon

The influence of wrinkling in reduced graphene oxide on their adsorption and catalytic properties

Song Bai [a], *Xiaoping Shen* [a,*], *Guoxing Zhu* [a], *Aihua Yuan* [b], *Jun Zhang* [b], *Zhenyuan Ji* [a], *Dezhou Qiu* [a]

[a] *School of Chemistry and Chemical Engineering, Jiangsu University, Zhenjiang 212013, China*
[b] *School of Biology and Chemical Engineering, Jiangsu University of Science and Technology, Zhenjiang 212003, China*

ARTICLE INFO

Article history:
Received 5 December 2012
Accepted 4 April 2013
Available online 10 April 2013

ABSTRACT

Reduced graphene oxide (RGO) with different amounts of wrinkling were synthesized in a water–ethylene glycol (EG) system with different volume ratios. The obtained RGO were characterized by X-ray powder diffraction, Raman spectroscopy, X-ray photoelectron spectroscopy, scanning and transmission electron microscopy, thermogravimetric analyze, and Brunauer–Emmett–Teller N_2 adsorption–desorption analysis. It was found that the degree of wrinkling decreased with an increase in the EG/water volume ratio. A possible mechanism for the formation of wrinkles was proposed. The adsorptive and catalytic properties of the RGO were investigated. Bare RGO were used to adsorb dyes as well as catalyze the reduction of 4-nitrophenol. The results revealed that neither the most wrinkled nor the smoothest RGO was best for the adsorptive and catalytic applications, while an intermediate state showed the best performance. A relationship between morphology, and the adsorptive and catalytic performance was discussed.

1. Introduction

Graphene, a two-dimensional (2D) material, composed of layers of carbon atoms packed into a honeycomb network, has attracted intense scientific interest mainly because of its large surface area and exceptional electrical, mechanical, thermal and optical properties [1–3]. Up-to-date, various methods have been developed for producing graphene. Among them, the method of sonication exfoliation-chemical reduction of graphene oxide (GO) into reduced graphene oxide (RGO) is both easily scalable and versatile in realizing abundant chemical functionalization and decoration [4,5]. However, the as-obtained RGO are different from the pristine graphene with the reason that the defects and oxygen-containing functional groups could not be removed completely during the reduction process [6]. In spite of this, RGO are widely used for the synthesis and practical application of graphene-based materials [7].

Wrinkles or ripples always exist in graphene in both experimental observation and theory simulations with the reason that perfect 2D crystals are thermodynamically unstable and cannot exist in the free smooth state, and the graphene become intrinsically stable by crumpling in the third dimension and minimizing the total free energy [8,9]. Wrinkling behavior has an important effect on the properties of graphene. For instance, Zheng et al. studied the effect of functional groups on the wrinkling properties of armchair graphene through molecular dynamics and molecular mechanics simulations [10]. Glukhova and Slepchenkov investigated the influence of the curvature of deformed graphene nanoribbons on their electronic and adsorptive properties based on the analysis of the local stress field for an atomic grid [11]. However,

* *Corresponding author:* Fax: +86 511 88791800.
E-mail address: xiaopingshen@163.com (X. Shen).
0008-6223/$ - see front matter
http://dx.doi.org/10.1016/j.carbon.2013.04.009

almost all of these researches are based on pristine graphene through theoretical investigation approach. In our previous works, smooth RGO and wrinkled RGO were used to fabricate hybrids for various applications, respectively [12,13]. Then the question is RGO, wrinkled or smooth, which is better? Obviously, it is also necessary to investigate the influence of wrinkling on the properties of RGO from an experimental viewpoint. However, so far, there has not been any report on the synthesis of RGO with different wrinkling.

Herein, we investigate the synthesis and properties of RGO with different amounts of wrinkling. The different wrinkling in RGO is achieved through changing the volume ratio of water to ethylene glycol (EG) in the reaction medium. With the removal of organic dye and reduction of 4-nitrophenol (4-NP) by $NaBH_4$ as model reactions, a systematic investigation into the adsorptive performance as well as catalytic activity of RGO with different wrinkling degree has been carried out. It is expected that this research presented here can provide some implications for the practical use of wrinkling in graphene-based materials for various applications.

2. Experimental

2.1. Materials

Natural flake graphite was purchased from Qingdao Guyu Graphite Co., Ltd. with a particle size of 150 μm. All other chemicals are of analytical grade and used without further purification.

2.2. Preparation of graphite oxide

Graphite oxide was synthesized from natural flake graphite by a modified Hummers method [14]. In a typical procedure, 2.0 g of graphite powder was added into cold (0 °C) concentrated H_2SO_4 (100 mL) solution containing $NaNO_3$ (4.0 g) in a 500 mL flask. Under vigorous stirring, $KMnO_4$ (10.0 g) was added gradually and the temperature of the mixture was kept below 10 °C. The reaction mixture was then stirred at 35 °C for 2 h until it became pasty brownish, and was diluted with de-ionized water (100 mL). When the addition of water, the reaction was cooled with an ice bath to keep the temperature below 100 °C, because the addition of water in concentrated H_2SO_4 medium violently released a large amount of heat. Then, the mixture was stirred for 30 min and 20 mL of 30 wt.% H_2O_2 was slowly added to the mixture to reduce the residual $KMnO_4$, after which the color of the mixture changed to brilliant yellow. The mixture was then filtered and washed with 5 wt.% HCl aqueous solution (800 mL) to remove metal ions followed by washing with 1.0 L of de-ionized water to remove the acid. For further purification, the as-obtained graphite oxide was re-dispersed in de-ionized water and then was dialyzed for one week to remove residual salts and acids. The resulted solid was centrifuged and dried at 60 °C for 24 h.

2.3. Preparation of RGO

The typical procedure for the preparation of RGO is as follows: 100 mg of graphite oxide was dispersed in 40 mL of water–EG mixed solvent by ultrasonication for 1 h. Then 2.0 mL of hydrazine hydrate was slowly added in. The mixture was stirred for 5 min, and then was transferred to a 50 mL Teflon-lined stainless steel autoclave and heated at 180 °C for 10 h. The resultant black product was isolated and washed with de-ionized water and ethanol several times by centrifugation, and finally dried at 45 °C in a vacuum oven. With the same procedure and the same amount of reaction reagents, various RGO were synthesized by adjusting the initial volume ratio of water to EG. The samples synthesized under different water–EG volume ratios were summarized in Table 1.

2.4. Characterization

The phase of the as-synthesized products was characterized using X-ray diffraction (XRD, Bruker D8 Advance diffractometer) with Cu Kα radiation (λ = 1.5406 Å) at a scanning rate of 4° min^{-1}. Raman spectra were carried out at room temperature using a DXR Raman microscope with 514.5 nm excitation source from an Ar^+ laser. The X-ray photoelectron spectroscopy (XPS) measurements were performed on a PHI 5000 VersaProbe. The morphology and size of the products were examined by transmission electron microscopy (TEM, JEOL JEM-2100) and field emission scanning electron microscopy (FESEM, JSM-7001). Thermogravimetric analyze (TGA) was conducted by an integrated thermal analyzer (STA 449C) with a heating rate of 10 °C min^{-1} under nitrogen atmosphere. The Brunauer–Emmett–Teller (BET) surface area of the RGO was tested using ASAP 2010 sorption analyzer. Ultraviolet–visible (UV–vis) spectroscopy measurements were performed on a UV-2450 UV–vis spectrophotometer.

2.5. Dye adsorptive experiment

Dye removal efficiency was determined by measuring the dye concentration before and after adsorption with constant stirring under ambient conditions. The initial concentration of dyes was 10 mg/L for methylene blue (MB) and rhodamine B (RhB), while the adsorbent concentration was 40 mg/L. For adsorption experiments, 4.0 mg of RGO was taken in 250 mL beaker and 100 mL of the dye solution was added. The mixture was sonicated for 1 min and then kept stirring. 2.0 mL of the dye solution was withdrawn at regular intervals, and their concentrations were determined by measuring the

Table 1 – Samples of RGO obtained with different water–EG volume ratio.

Samples	RGO-1	RGO-2	RGO-3	RGO-4	RGO-5	RGO-6
Water–EG volume ratio	40:0	20:20	10:30	5:35	2.5:37.5	0:40

absorbance of the solutions at 664 nm for MB and 554 nm for RhB with the UV–vis spectrophotometer. The adsorption amount (q_t, mg/g) can be calculated by the mass balance equation as follows:

$$q_t = \frac{(C_0 - C_t)V}{m} \quad (1)$$

where C_0 (mg/L) is the initial dye concentration before removal, C_t (mg/L) is the concentration of dye at time t, V (L) is the volume of the aqueous solution, and m is the weight of the RGO adsorbents.

2.6. Catalytic reduction of 4-NP

In a typical reaction, 1.0 mL of 4-NP aqueous solution (5.0 mM) was added into 100 mL of de-ionized water. A freshly prepared aqueous solution of $NaBH_4$ (2.0 mL, 3.0 M) was added in, leading to a color change from light yellow to yellow green. Then the as-obtained solution was added into a 250 mL beaker containing 10.0 mg of a catalyst to start the reaction, and the reaction solution was kept stirring. During the reaction process, 2.0 mL of the reaction solution was withdrawn at a given time interval, which was immediately recorded in the UV–vis spectrophotometer in a scanning range of 200–600 nm at ambient temperature.

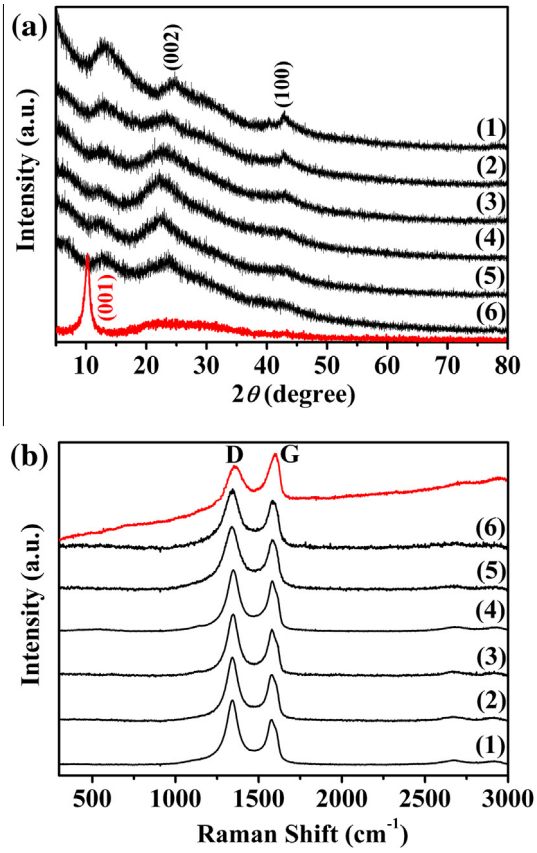

Fig. 1 – (a) XRD patterns and (b) Raman spectra of (1) RGO-1, (2) RGO-2, (3) RGO-3, (4) RGO-4, (5) RGO-5, (6) RGO-6 as well as graphite oxide (red lines). (For interpretation of the references to color in this figure legend, the reader is referred to the web version of this article.)

3. Results and discussion

3.1. Characterization of RGO

The RGO were solvothermally synthesized by reduction of GO nanosheets with hydrazine hydrate in a water–EG system. With the increasing volume ratio of EG in the reaction system from 0% to 100%, the RGO samples from RGO-1 to RGO-6 were synthesized. The XRD patterns of the as-synthesized RGO as well as graphite oxide are shown in Fig. 1a. Compared with the pattern of graphite oxide, the strong (001) peak centered at $2\theta = 10.2°$ disappears in the diffraction patterns of RGO, confirming that graphite oxide has been flaked and reduced [15]. The as-obtained RGO (RGO-1–RGO-6) show a broad (002) peak at 2θ of 24.2°, 23.3°, 22.8°, 22.1°, 22.7° and 23.6°, respectively, corresponding to the d-spacing of 0.36, 0.38, 0.39, 0.40, 0.39 and 0.37 nm, respectively. All the d-spacings of RGO are larger than that of pristine graphite (0.34 nm), which may be due to the irregular stacking of wrinkled graphene. From RGO-1 to RGO-6, it was also found that the d-spacing increased firstly, and then decreased. Another peak with 2θ at about 42.5° was also observed, corresponding to its (100) reflection. It should be noted that the relative peak sharpness of the (100) peak decreases from RGO-1 to RGO-6, showing the decline of graphitization degree [16].

Fig. 1b shows the Raman spectra of the as-obtained RGO as well as graphite oxide, which display two prominent peaks, corresponding to the well-documented D and G bands, respectively. The D band is associated with the defects, while the G band corresponds to the graphitic band related to the order of the sample [17]. Graphite oxide displays the D band and G band at 1357 and 1600 cm^{-1}, respectively, while pristine graphite shows G band at 1575 cm^{-1} [18]. This difference was attributed to the presence of isolated double bonds in GO, which resonate at frequencies higher than that of the G band of the graphite [19]. For RGO, the D band is located at about 1344 cm^{-1}, while the G band shifts upward from the 1575 cm^{-1} of RGO-1 to 1585 cm^{-1} of RGO-6 (1577, 1579, 1582 and 1584 cm^{-1} for RGO-2, RGO-3, RGO-4 and RGO-5, respectively), which is more and more far from the value of pristine graphite, corresponding to the decrease in the recovery of the hexagonal network of carbon atoms, once again confirming the decline in the degree of graphitization from RGO-1 to RGO-6 [20–23]. In addition, the integrated intensity ratio of the D and G band (I_D/I_G) for RGO shows an enhanced value ($I_D/I_G \geqslant 1.3$) in comparison with graphite oxide ($I_D/I_G = 0.95$), indicating more sp^2 domains were formed during the reduction of GO [24].

The C 1s XPS spectra of as-obtained RGO as well as graphite oxide are shown in Fig. 2. The deconvolution spectra show four different peaks centered at 284.6, 286.4, 287.8 and 289.0 eV, corresponding to C–C, C–O, C=O and O=C–O groups, respectively [25]. In comparison with the C 1s spectra of graphite oxide, the intensities of C–O, C=O and O=C–O peaks decrease significantly, confirming the effective removal of

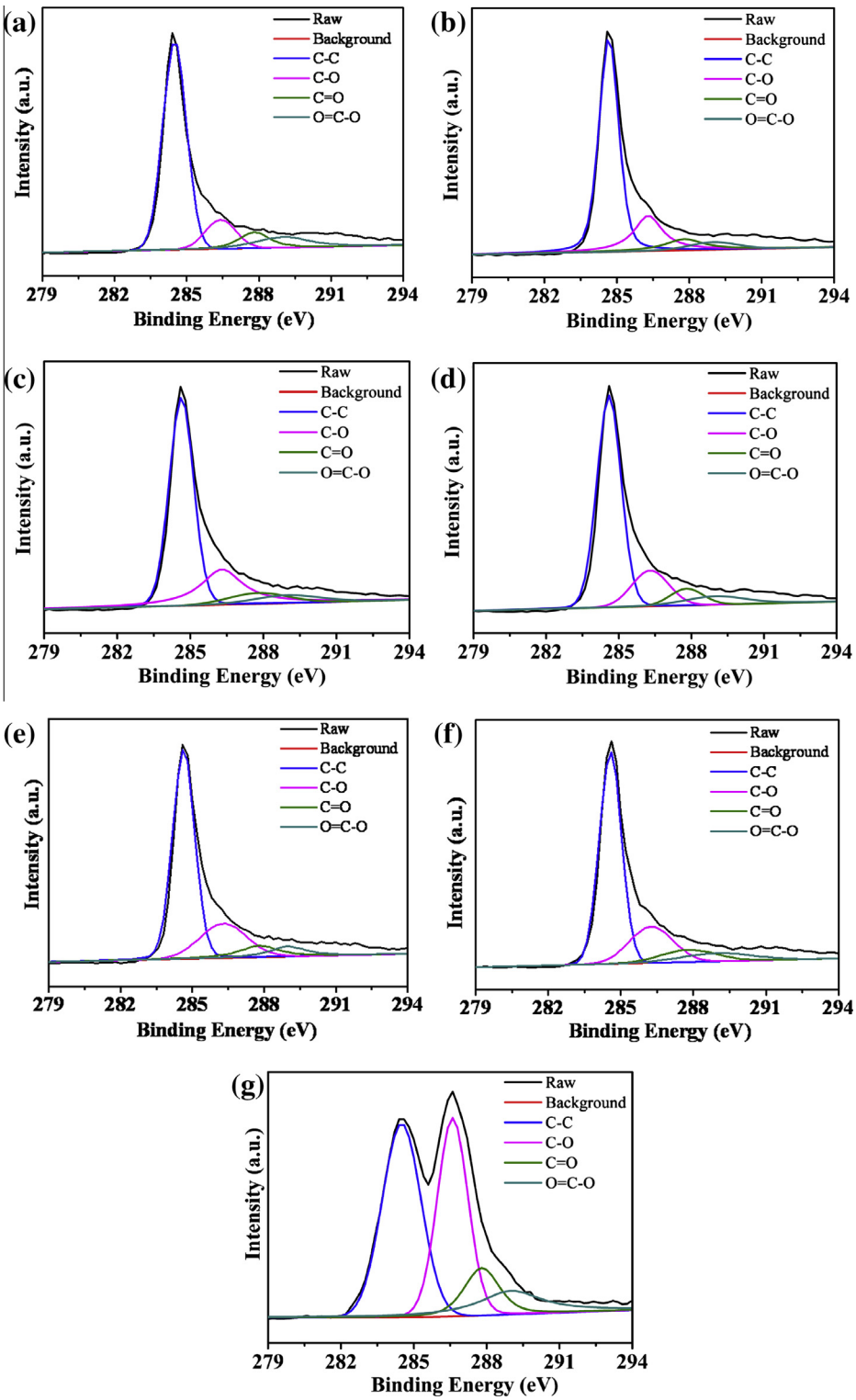

Fig. 2 – C 1s XPS spectra of (a) RGO-1, (b) RGO-2, (c) RGO-3, (d) RGO-4, (e) RGO-5, (f) RGO-6 as well as (g) graphite oxide.

oxygen-containing functional groups and the high reduction degree of RGO. The C 1s spectra of the different RGO look much similar with the reason that the same amount of strong reducing agent was added. However, when observed carefully, it could be found that the intensity of C 1s peaks from the carbon binding to oxygen shows a slight increase from RGO-1 to RGO-6 (peak area ratio of C–O, C=O, O=C–O bonds to C–C bond for RGO-1, RGO-2, RGO-3, RGO-4, RGO-5 and RGO-6 is 0.39, 0.41, 0.46, 0.48, 0.54, and 0.56, respectively), suggesting a little decline in deoxygenation degree of RGO. There is no difference in the O 1s peaks among the different RGO samples (Fig. S1). They are located at 531.8 eV, corresponding to the remaining O–C bond [26]. But their intensities were much lower than the O 1s peak of graphite oxide (Fig. S1). Also

from the XPS data, the C/O molar ratio of RGO-1, RGO-2, RGO-3, RGO-4, RGO-5 and RGO-6 was 17.94, 15.18, 12.35, 11.32, 11.02 and 10.63, respectively, showing the trend of decrease. Naturally, these values are much larger than the C/O molar ratio (2.25) of graphite oxide. These results agree well with the decline of graphitization degree from RGO-1 to RGO-6 due to the deoxygenation function of the graphitization process [27,28].

The morphology of the as-synthesized RGO was characterized by FESEM and TEM (Fig. 3). From the FESEM images, it can be clearly seen that many RGO nanosheets closely associate with each other in all the samples. Meanwhile, these RGO samples show different morphology on the whole. Among them, the RGO-1 and RGO-2 show the highest degree of wrinkling, which aggregated severely into flower petal-like shapes. From the TEM images, it can be seen that the wrinkles with high amplitude/wavelength aspect ratio in RGO-1 and RGO-2 are much clear, and the fold lines within the nanosheets are very long and thick. On the contrary, the RGO-6 show the lowest degree of wrinkling. The nanosheets are very flat and smooth, and the fold lines on them are vague. The TEM and FESEM images of RGO-3, RGO-4 and RGO-5 exhibit that the wrinkling situation of them falls in between RGO-2 and RGO-6, and the wrinkling degree gradually decreases from RGO-3 to RGO-5, revealing that the degree of wrinkling decreases with the increasing volume ratio of EG in the reaction medium. Furthermore, considering the distinctive morphology of RGO-6 as compared with other RGO samples, it could be concluded that water plays an important role in the formation of wrinkles on RGO.

To investigate the formation mechanism of wrinkles on RGO, it is firstly needed to determine when the wrinkles are formed. FESEM images (Fig. 4a and b) shows that no apparent wrinkle exists in the graphite oxide. After the graphite oxide was dispersed into pure water through ultrasonication, the obtained GO nanosheets do not show apparent wrinkles as shown in the TEM images (Fig. 4c and d), revealing that the wrinkles were not formed in the ultrasonic process. Therefore, it can be reasonably inferred that the followed solvothermal-reduction process should be responsible for the

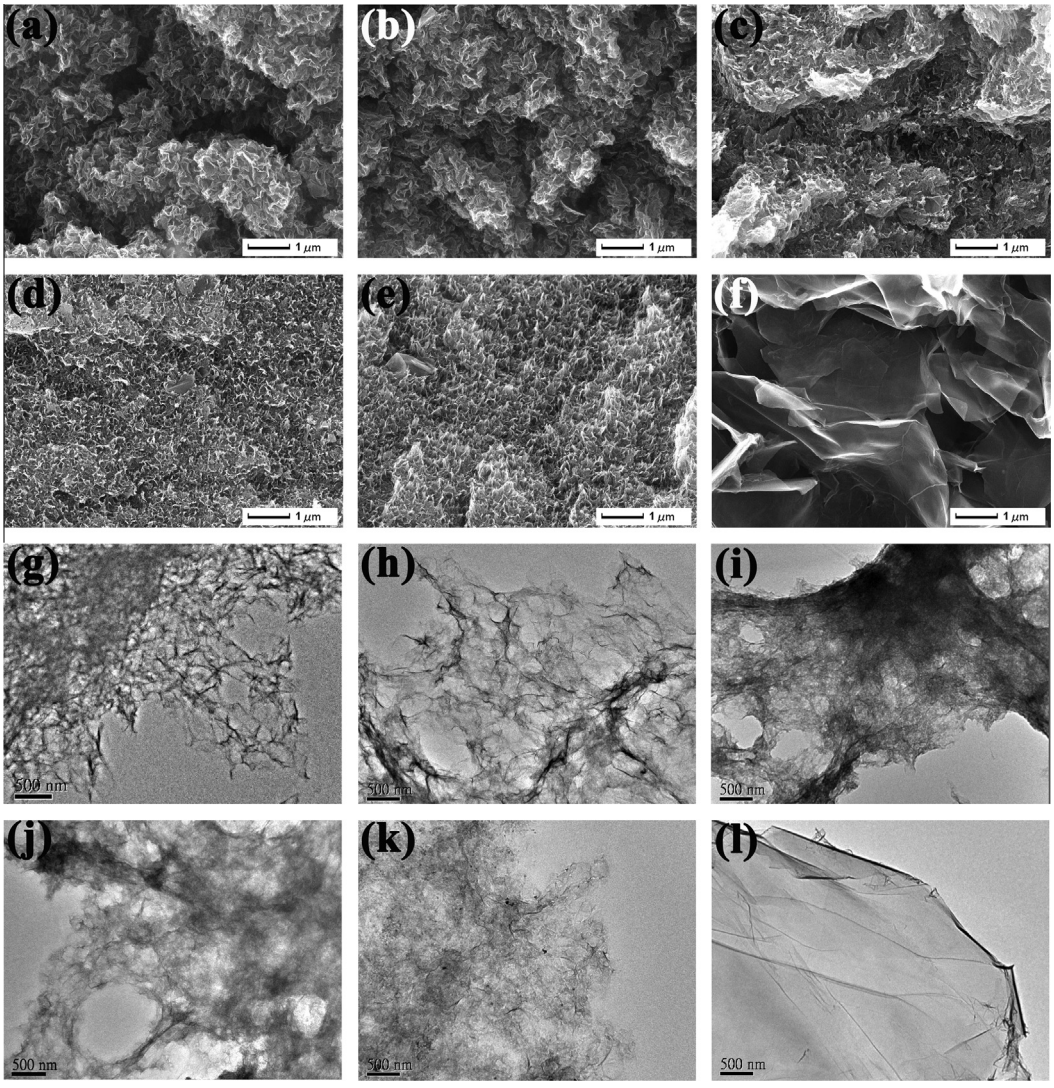

Fig. 3 – FESEM and TEM images of (a, g) RGO-1; (b, h) RGO-2; (c, i) RGO-3; (d, j) RGO-4; (e, k) RGO-5 and (f, l) RGO-6, respectively.

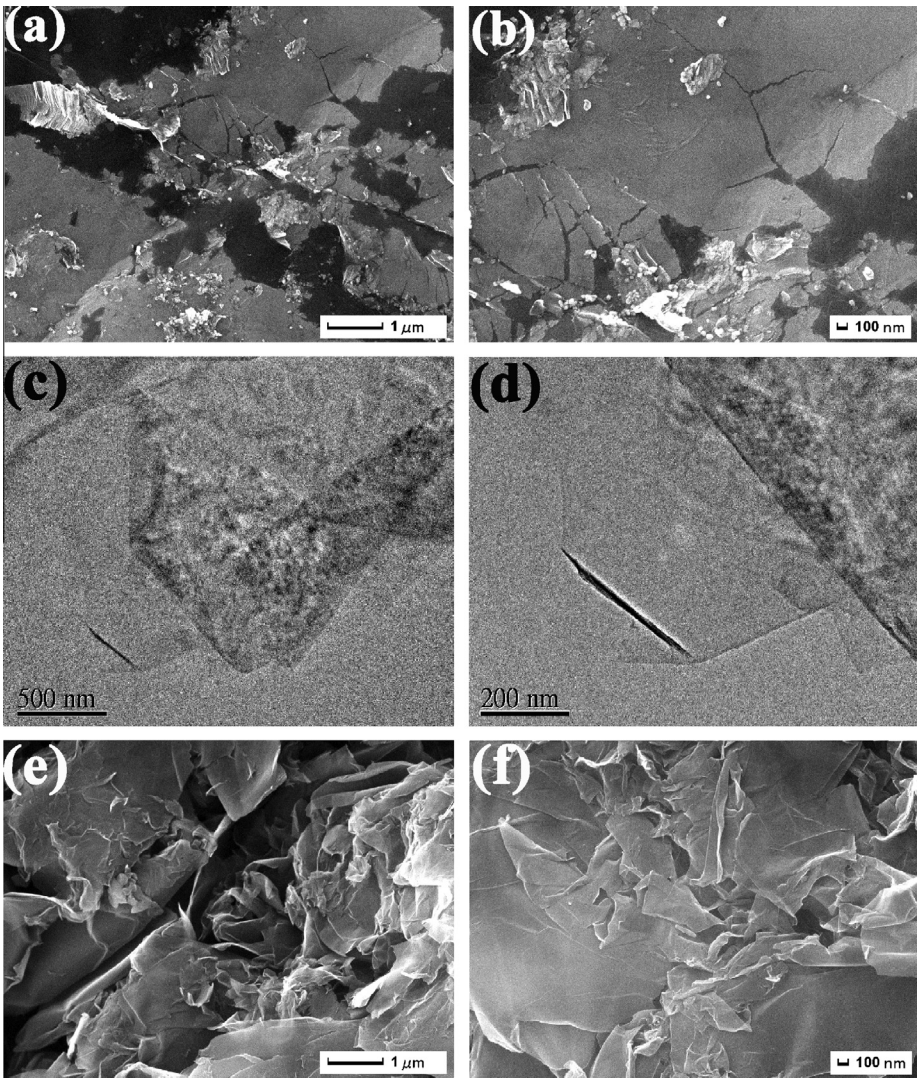

Fig. 4 – (a, b) FESEM images of graphite oxide, (c, d) TEM images of GO nanosheets dispersed in water, (e, f) FESEM images of RGO nanosheets obtained in water/PVP system (water: 40 mL; PVP K30: 4 g).

formation of the wrinkles. As an analogous case, it has been reported that flake-like GO can be reflux-reduced to crumpled RGO in a water/ethanol system [29]. We consider that in the heating process, the heat energy decreases the stability of the 2D nanosheets, resulting in the crumpling of them through bending or buckling. On the other hand, with the reduction of GO into RGO, the rich functional groups on them are removed, which also reduces their thermodynamic stability.

Then the question is why EG in the solvent can restrain the formation of wrinkles on RGO. Paredes et al. have shown that through sonication, both water and EG as solvent can fully exfoliate graphite oxide and disperse the as-obtained GO nanosheets well [30]. We believe that the higher viscosity of EG may contribute to the lower wrinkling degree of RGO. Viscosity is a measure of the resistance to fluid deformation. In the reduction process, whether through hydrothermal/solvothermal route or reflux approach, the deformation of solvents results from the high temperature, high pressure or stirring can also drive the deformation of RGO nanosheets. The deformation of RGO in EG with higher viscosity would endure bigger obstruction than in water and thus leads to relatively low wrinkling. Moreover, high viscosity decreases the diffusion rate of GO nanosheets in EG during the reduction process [31], thus the chance of collision, overlapping and cross-linking of flexible RGO nanosheets, which would lead to the deformation of RGO, could be reduced [32]. This can be supported by FESEM images (Fig. 4e and f) of the RGO synthesized in a water/PVP system under the same experimental condition, in which PVP increases the viscosity of the solvent and thus alleviates the degree of wrinkling. Another possible reason may be the larger heat capacity of water in comparison with EG. Water as a solvent can absorb more quantity of heat during the heat-reduction process when heating up to the same temperature (180 °C), which leads to the increase of the instability of RGO nanosheets and, as a result, the higher degree of wrinkling formed. More quantity of heat may also cause the higher graphitization degree of RGO. It was reported that graphitization and deoxygenation can cause the shrinkage of RGO agglomerations [27].

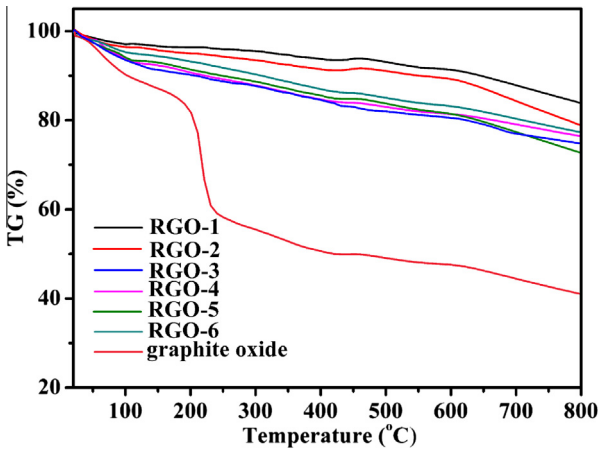

Fig. 5 – TGA curves of the obtained RGO as well as graphite oxide.

The TGA curves of as-obtained RGO as well as graphite oxide under nitrogen flow are shown in Fig. 5. For graphite oxide, there is a small weight loss (below 100 °C) and a major weight loss (180–240 °C), corresponding to the loss of adsorbed water and pyrolysis of labile oxygen-containing functional groups, respectively [33]. In contrast, TGA curves of RGO only exhibit slight weight loss below 100 °C, showing the removal of oxygen-containing functional groups as well as relatively low and approximate water content of various RGO. Moreover, RGO-1 and RGO-2 show better thermal stability in comparison with the others, corresponding to their higher graphitization degree.

Nitrogen adsorption and desorption measurements are used to further estimate the inner structures of RGO. The nitrogen adsorption and desorption isotherm curves of the obtained RGO are shown in Fig. 6a. The shape of the isotherms indicates that the RGO contain both micro and mesopores [24]. Moreover, it can be clearly seen that the hysteresis loops of RGO-1 and RGO-2 are much broader than those of other RGO, showing the existence of many large pores in highly crumpled RGO. The BET specific surface area of the samples from RGO-1 to RGO-6 is calculated to be 427.2, 836.9, 1004.3, 662.7, 57.6 and 36.2 m^2/g, respectively. The value of RGO-1 is much larger than that of RGO-6, showing that the surface area of wrinkled RGO is larger than that of flat RGO. The curve of the change in BET surface area from RGO-1 to RGO-6 is shown in Fig. 6b. It can be seen clearly that the surface area increases from RGO-1 to the largest of RGO-3, and then decreases to the smallest of RGO-6. This agrees with the change trend in the *d*-spacing of RGO, displaying the relationship between the BET surface area and the *d*-spacing. It is believed that there is an optimum wrinkling degree for the biggest surface area. If the graphene sheets are highly wrinkled, which are just like agglomeration within one RGO nanosheet, it will obviously decrease the *d*-spacing and surface area. On the other hand, flat RGO without wrinkling incline to restack, forming graphite structure and causing smaller surface area. It seems that the different restacking behaviors of RGO nanosheets with different wrinkling have a bigger influence on their surface area. It is also worth to point out that the irreversible agglomeration has happened in all of the RGO samples during the reduction process with the reason of their hydrophobicity. So the restacking behaviors of RGO samples in dry condition could not change when they are dispersed in water. This could be supported by the poor dispersibility of RGO in water with different pH values (Fig. S2).

3.2. *Adsorption properties of RGO*

RGO-based materials are well known as adsorbents for dyes due to the layered nature and large surface area of RGO. Moreover, the π–π stacking between aromatic structure of dyes and sp^2 regions of RGO, as well as the electrostatic interactions between charged dye and the surface oxygen-containing groups of RGO may also assist in the adsorption of dyes [34]. The adsorption behavior of the RGO with different wrinkling degree was probed through the adsorption of MB and RhB with the dye concentration of 10 mg/L and RGO concentration of 40 mg/L. After the addition of adsorbents, the concentration of the dyes decreased in the process of time (Fig. 7a and b). The time-dependent removal efficiency curves of MB and RhB are shown in Fig. 7c and d, respectively. For all adsorbents, it can be seen that the increase of the removal efficiency is rapid at the beginning and then gradually slows down with the prolongation of the adsorption time. However, the detailed adsorption behavior of these RGO samples is not identical. For RGO-1, RGO-2, and RGO-3 with heavy wrinkles, the removal efficiency of the dyes keeps increasing even

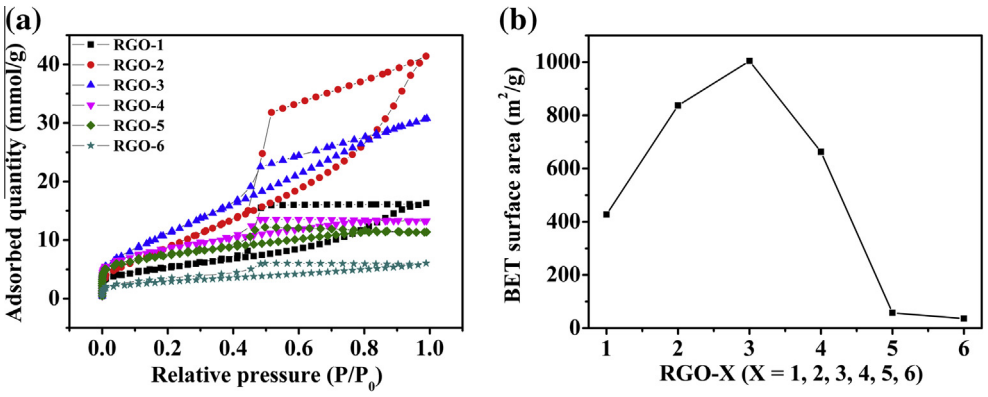

Fig. 6 – (a) N_2 adsorption–desorption isotherms and (b) the BET specific surface area of the obtained RGO.

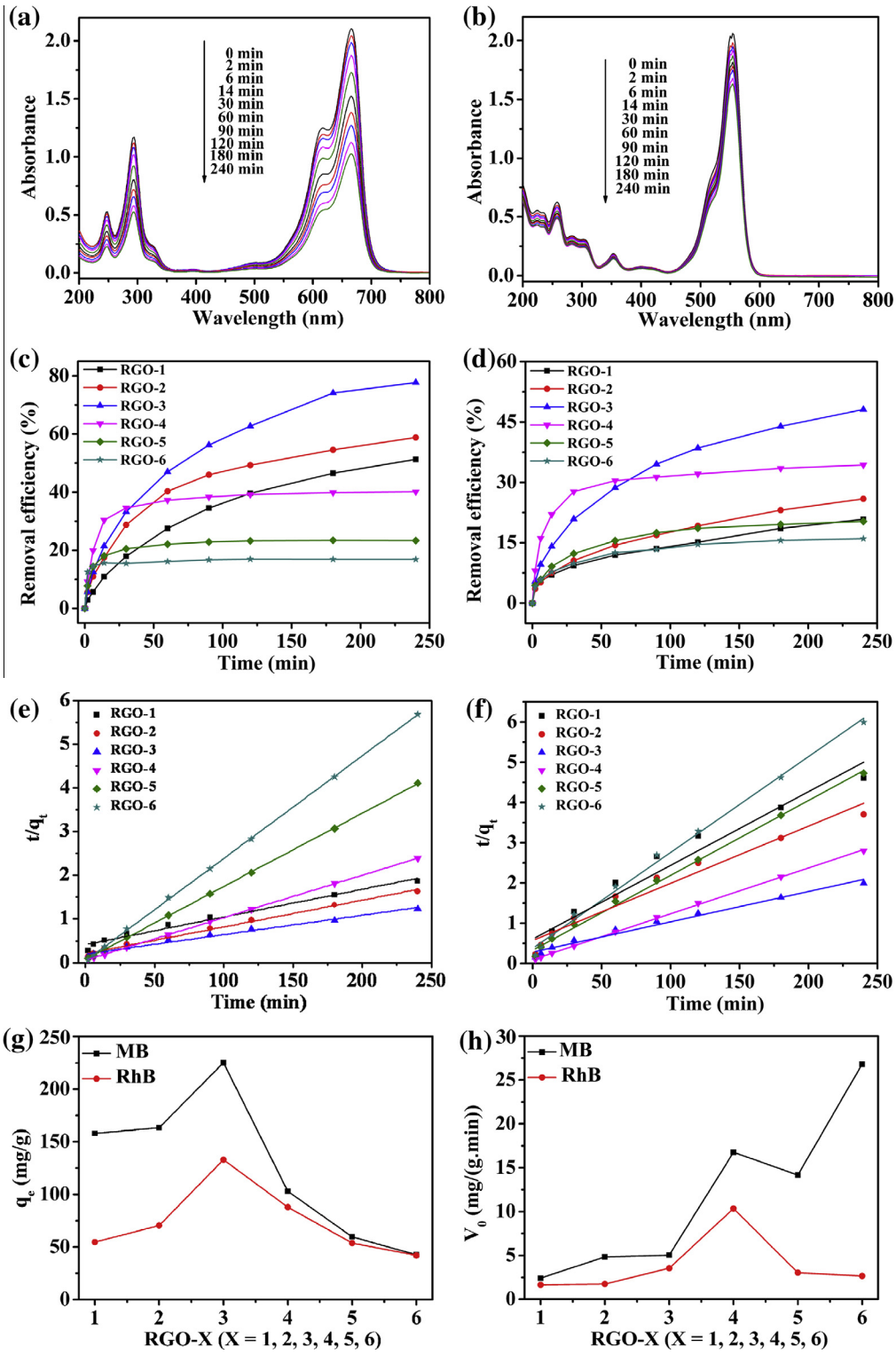

Fig. 7 – UV–vis absorption spectra of the MB (a) and RhB (b) with RGO-1 as absorbent. Removal efficiency of (c) MB and (d) RhB on RGO, pseudo-second-order kinetic plots for the adsorption of (e) MB and (f) RhB on RGO, and the corresponding kinetic parameters (g) q_e and (h) V_0 of the RGO samples for MB and RhB adsorption. The initial concentration of dye solution was 10 mg/L and the concentration of RGO was 40 mg/L.

when the adsorption time is up to 4 h. While for RGO-4, RGO-5 and RGO-6 with less wrinkles, the increase of the removal efficiency is not obvious when the adsorption time is more than 1 h, suggesting that the adsorption tends to saturation. This indicates that the wrinkles in graphene sheets contribute to durative adsorption performance of RGO. With 4 h

adsorption, the removal efficiency of MB decreases in the following order: RGO-3 > RGO-2 > RGO-1 > RGO-4 > RGO-5 > RGO-6. We also find that the adsorption efficiency of RGO to RhB is much lower than that to MB, making the advantage of high wrinkling RGO over low wrinkling RGO not too obvious in RhB removal in a relatively short adsorption time (4 h). From the removal efficiency curves, it is also observed that in the first 14 min adsorption, the RGO-4 shows the highest adsorption efficiency, while the RGO-1 shows the lowest adsorption efficiency, indicating that RGO with heavy wrinkling may have a relatively low initial adsorption rate.

In our previous work, it was found that RGO-based materials followed the pseudo-second-order kinetics nature in the adsorption processes [35]. So here we use pesudo-second-order model to analyze the adsorption kinetics of the RGO, which is defined as follows:

$$\frac{t}{q_t} = \frac{1}{k_2 q_e^2} + \frac{t}{q_e} \quad (2)$$

where q_e (mg/g) is the adsorption capacity at equilibrium and q_t is the adsorption amount of dye at time t. The parameter k_2 (g/(mg min)) represents the pseudo-second-order rate constant of the kinetic model. The slope and intercept of the linear plot of t/q_t against t yield the values of q_e and k_2. Additionally, the initial adsorption rate V_0 (mg/(g min)) can be determined from the Equation:

$$V_0 = k_2 q_e^2 \quad (3)$$

The plots of t/q_t versus t for MB and RhB are given in Fig. 7e and f, respectively, and the parameter of q_e (mg/g), k_2 (g/(mg min)), V_0 (mg/(g min)), and correlation coefficients (R^2) are also shown (Table S1). It can be seen that low wrinkling RGO (RGO-4, RGO-5 and RGO-6) show good linearity of the plots ($R^2 > 0.995$), revealing the good agreement between experimental and calculated q_e values. But for high wrinkling RGO (RGO-1, RGO-2 and RGO-3), the plots have relatively poor linearity and the values of R^2 are relatively low. For each of the RGO samples, the value of q_e for MB is larger than that for RhB. For both MB and RhB, the q_e values of the RGO samples show an increase from RGO-1 to RGO-3, and then a decrease from RGO-3 to RGO-6 (Fig. 7g). Thus RGO-3 and RGO-6 show the largest and smallest values of q_e, respectively, which correspond to the largest BET surface area of RGO-3 and the smallest one of RGO-6. Moreover, from RGO-1 to RGO-6, the change in the value of q_e matches well with the BET surface area, confirming the positive correlation between them. The change of the value V_0 from RGO-1 to RGO-6 also confirms the high and low initial adsorption rate of RGO-4 and RGO-1, respectively, as well as the relatively high initial adsorption rate of RGO with low wrinkling (Fig. 7h). Moreover, the recycling of RGO in the removal of dyes could be realized with the reason that the RGO could be separated and the desorption of dyes from RGO could be happened when ethylene glycol (EG) was added in (Fig. S3).

Due to the high and similar reduction degree of different RGO (Fig. 2), the π–π and electrostatic interactions between dyes and various RGO may not contribute to the different adsorption performance. We believe that the different stacking structure (Fig. 3) of RGO due to their different wrinkling degree as well as the resulting different micropore/mesopore distribution in them may be the true reason. This could be further confirmed by the adsorption performance of pristine flake graphite as well as pure GO nanosheets (Fig. S4). The flake graphite shows very low removal efficiency due to the tight stacking of flat graphene leading to few micropores/mesopores; while for GO, smooth nanosheets were fully exfoliated and dispersed in water, and no micropore/mesopore was produced. So GO shows a high initial adsorption rate but reaches its saturation point at a very early stage. Of course, its high adsorption efficiency was mainly due to large surface area and the large amount of oxygen-containing groups of GO.

3.3. *Catalytic properties of RGO*

It has been reported that RGO could be used as catalysts in some organic reactions, such as hydrogenation of nitrobenzene [36] and oxidation of organic pollutants [37]. The catalytic mechanism could be attributed to the zigzag edges of RGO, which act as catalytic active sites to facilitate the activation of reactant molecules [36,37]. Moreover, the strong adsorption capability of RGO as well as the π–π stacking interaction between the organic molecules and RGO was believed to enhance the catalytic activities. Herein, the catalytic properties of the RGO were evaluated with the reduction of 4-NP into 4-aminophenol (4-AP) by $NaBH_4$. As far as we know, there are few reports on the catalytic activity of bare RGO in reduction of 4-NP. The reactions were monitored by the time-dependent UV–vis absorption spectra. When 4-NP was mixed with an excess amount of $NaBH_4$, the mixture showed a strong absorption peak at 400 nm. With the addition of RGO catalysts, the absorption peak at 400 nm gradually dropped in intensity as the reduction reaction proceeded. Meanwhile, a new peak at 300 nm started to rise with the production of 4-AP (Fig. 8) [38]. The catalytic activity of RGO was clearly confirmed when we compared the UV–vis spectra in Fig. 6 with the absorption spectra of 4-NP with no catalyst added (Fig. S5a), in which the peak at 400 nm does not apparently drop even after 3 h. From Fig. 8a–f, it can be seen that the RGO-4 and RGO-5 show high catalytic activity with about 35 min to finish the reaction, while RGO-1 exhibits the lowest catalytic activity and only about half of the amount of 4-NP was reduced with reaction time of 140 min.

It is proposed that the rate of the reduction reaction is independent of the concentration of $NaBH_4$ and the reaction follows the pseudo-first-order kinetics with respect to the concentration of 4-NP [39]. Fig. 8g shows the plots of $\ln(C_t/C_0)$ (C_t and C_0 are 4-NP concentrations at time t and 0, respectively) versus time t obtained based on the absorbance as the function of time. Good linear correlations ($R^2 > 0.97$) of the plots are observed for the RGO catalysts, confirming the pseudo-first-order nature of the reaction. From the slopes of the plots, the apparent rate constants (k_{app}) can be obtained. The values of k_{app} for different RGO catalysts are shown in Fig. 8h, which shows that the catalytic activities decrease in the following order: RGO-4 > RGO-5 > RGO-6 > RGO-3 > RGO-2 > RGO-1, suggesting that the RGO with high wrinkling degree show relatively low catalytic activities. This result is in contrast with the adsorption performance, in which RGO with high wrinkling degree display good adsorption performance,

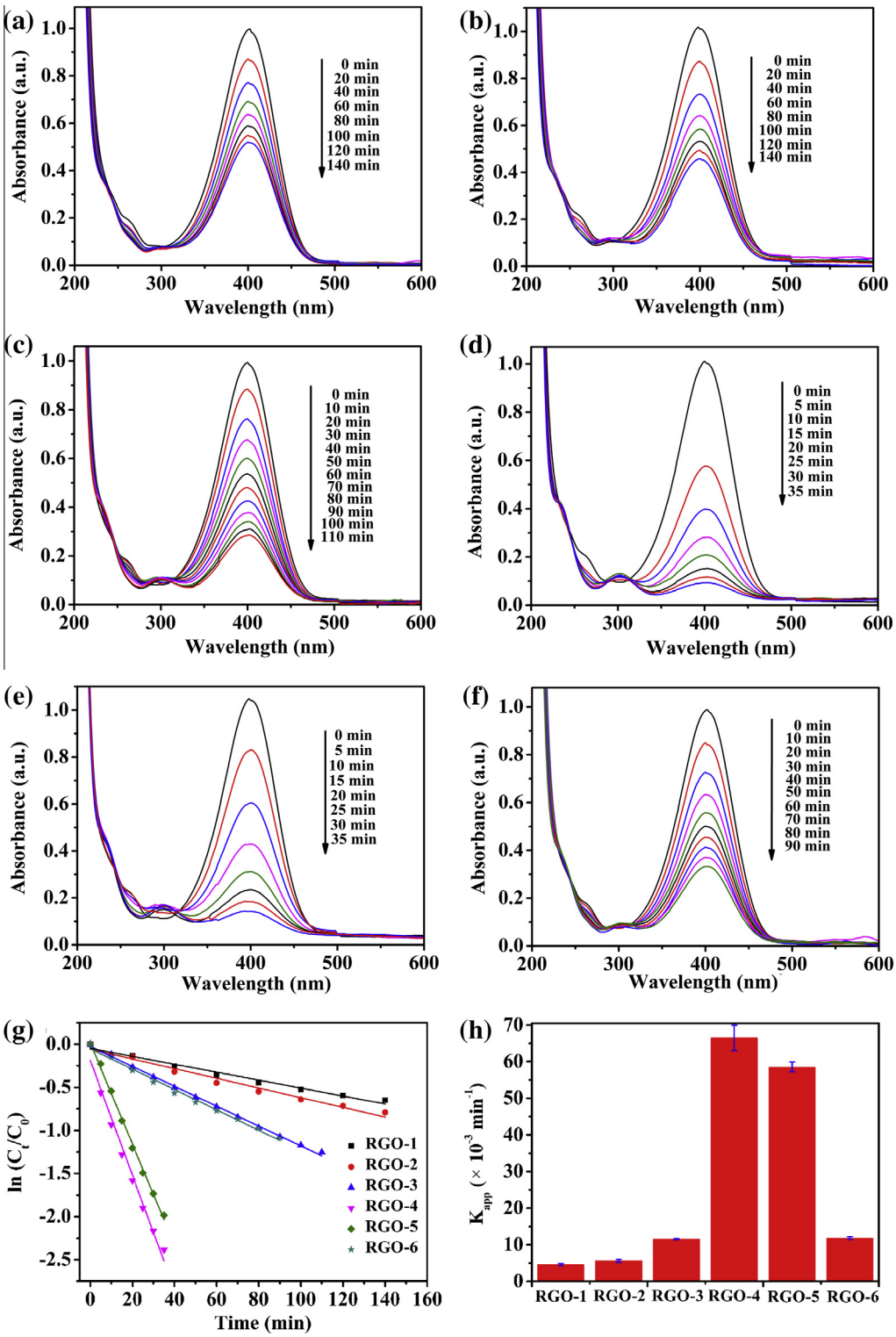

Fig. 8 – UV–vis absorption spectra of the reduction of 4-NP by $NaBH_4$ in the presence of RGO catalyst: (a) RGO-1; (b) RGO-2; (c) RGO-3; (d) RGO-4; (e) RGO-5 and (f) RGO-6. (g) Plots of $\ln(C_t/C_0)$ of 4-NP versus reaction time for the RGO catalysts. (h) Values of k_{app} with different RGO as catalysts. The error bars in (h) represent the standard errors of the slopes in the plots.

revealing that high adsorption performance did not necessarily result in high catalytic activity. In spite of this, we found that RGO-4 with the highest adsorption rate in the first 14 min also showed the highest catalytic activity in the initial 15 min (Fig. 8d), while RGO-1 with the lowest initial adsorption rate exhibited the lowest initial catalytic activity (Fig. 8a), indicating the correlation between initial adsorption rate and initial catalytic activity. What's more interesting is that the values of k_{app} also increased firstly from RGO-1 to RGO-4, and then decreased from RGO-4 to RGO-6. This change

trend is similar to the changes in the BET surface area and in the value of q_e, showing that neither the most wrinkled nor the smoothest RGO but an intermediate state shows the best performance in various properties and applications.

For comparison, the catalytic properties of pristine flake graphite and pure GO in the reduction of 4-NP were also investigated. The flake graphite shows very low catalytic activity (Fig. S5b); while for GO, its UV–vis absorption spectrum overlaps with that of 4-NP. Moreover, the absorbance at 400 nm increases rather than decreases as time goes on, and thus no catalytic activity was observed for GO (Fig. S5c). All of these demonstrate that RGO with zigzag edges is a unique metal-free catalyst for the reduction process.

4. Summary

RGO with different degree of wrinkling have been synthesized through solvothermal reduction of GO in a water–EG system. The wrinkling degree of the as-synthesized RGO decreases with the increasing volume ratio of EG to water. The influence of EG/water volume ratio on the wrinkling of RGO would be related to the different viscosity and heat capacity between water and EG. EG with higher viscosity restrains the deformation of RGO; meanwhile, EG with lower heat capacity increases the thermostability of RGO. It is found that the RGO with different wrinkling degree show different performances in the adsorption of organic dyes and catalytic reduction of 4-NP. It is interesting that neither the most wrinkled nor the smoothest RGO but an intermediate one shows the best performance in the adsorption and catalysis applications. Furthermore, the relationship between morphology, and the BET surface area, adsorptive and catalytic performances of the RGO is clearly revealed.

Acknowledgements

The authors are grateful for financial support from the National Natural Science Foundation of China (Nos. 51272094 and 51072071).

Appendix A. Supplementary data

Supplementary data associated with this article can be found, in the online version, at http://dx.doi.org/10.1016/j.carbon.2013.04.009.

REFERENCES

[1] Li D, Kaner RB. Materials science – graphene-based materials. Science 2008;320:1170–1.
[2] Geim AK, Novoselov KS. The rise of graphene. Nat Mater 2007;6:183–91.
[3] Rao CNR, Sood AK, Subrahmanyam KS, Govindaraj A. Graphene: the new two-dimensional nanomaterial. Angew Chem Int Ed 2009;48:7752–77.
[4] Park S, Ruoff RS. Chemical methods for the production of graphenes. Nat Nanotechnol 2009;4:217–24.
[5] Bai S, Shen XP, Zhu GX, Xu Z, Liu YJ. Reversible phase transfer of graphene oxide and its use in the synthesis of graphene-based hybrid materials. Carbon 2011;49:4563–70.
[6] Guo SJ, Dong SJ. Graphene nanosheet: synthesis, molecular engineering, thin film, hybrids, and energy and analytical applications. Chem Soc Rev 2011;40:2644–72.
[7] Bai S, Shen XP. Graphene-inorganic nanocomposites. RSC Adv 2012;2:64–98.
[8] Meyer JC, Geim AK, Katsnelson MI, Novoselov KS, Booth TJ, Roth S. The structure of suspended graphene sheets. Nature 2007;446:60–3.
[9] Wang CY, Mylvaganam K, Zhang LC. Wrinkling of monolayer graphene: a study by molecular dynamics and continuum plate theory. Phys Rev B 2009;80:155445.
[10] Zheng QB, Geng Y, Wang SJ, Li ZG, Kim JK. Effects of functional groups on the mechanical and wrinkling properties of graphene sheets. Carbon 2010;48:4315–22.
[11] Glukhova O, Slepchenkov M. Influence of the curvature of deformed graphene nanoribbons on their electronic and adsorptive properties: theoretical investigation based on the analysis of the local stress field for an atomic grid. Nanoscale 2012;4:3335–44.
[12] Bai S, Shen XP, Zhu GX, Xu Z, Yang J. In situ growth of FeNi alloy nanoflowers on reduced graphene oxide nanosheets and their magnetic properties. CrystEngComm 2012;14:1432–8.
[13] Bai S, Chen SQ, Shen XP, Zhu GX, Wang GX. Nanocomposites of hematite (α-Fe_2O_3) nanospindles with crumpled reduced graphene oxide nanosheets as high-performance anode material for lithiumion batteries. RSC Adv 2012;2:10977–84.
[14] Hummers WS, Offeman RE. Preparation of graphitic oxide. J Am Chem Soc 1958;80. 1339–9.
[15] Zhu CZ, Guo SJ, Fang YX, Dong SJ. Reducing sugar: new functional molecules for the green synthesis of graphene nanosheets. ACS Nano 2010;4:2429–37.
[16] Fujimoto H. A new estimation method for the degree of graphitization for random layer lattices. Carbon 2010;48:3446–53.
[17] Ferrari AC, Meyer JC, Scardaci V, Casiraghi C, Lazzeri M, Mauri F, et al. Raman spectrum of graphene and graphene layers. Phys Rev Lett 2006;97:187401.
[18] Tuinstra F, Koenig JL. Raman spectrum of graphite. J Chem Phys 1970;53:1126–30.
[19] Ferrari AC, Robertson J. Interpretation of Raman spectra of disordered and amorphous carbon. Phys Rev B 2000;61:14095–107.
[20] Moon IK, Lee J, Ruoff RS, Lee H. Reduced graphene oxide by chemical graphitization. Nat Commun 2010;1:73.
[21] Su CY, Xu YP, Zhang WJ, Zhao JW, Liu AP, Tang XH, et al. Highly efficient restoration of graphitic structure in graphene oxide using alcohol vapors. ACS Nano 2010;4:5285–92.
[22] Kudin KN, Ozbas B, Schniepp HC, Prudhomme RK, Aksay IA, Car R. Raman spectra of graphite oxide and functionalized graphene sheets. Nano Lett 2008;8:36–41.
[23] Chen WF, Yan LF, Bangal PR. Chemical reduction of graphene oxide to graphene by sulfur-containing compounds. J Phys Chem C 2010;114:19885–90.
[24] Stankovich S, Dikin DA, Piner RD, Kohlhaas KA, Kleinhammes A, Jia Y, et al. Synthesis of graphene-based nanosheets via chemical reduction of exfoliated graphite oxide. Carbon 2007;45:1558–65.
[25] Bai S, Shen XP, Zhu GX, Zhou H, Xu H, Fu GH, et al. Optical properties and a simple and general route for the rapid syntheses of reduced graphene oxide–metal sulfide nanocomposites. Eur J Inorg Chem 2013:256–62.
[26] Yang D, Velamakanni A, Bozoklu G, Park S, Stoller M, Piner RD, et al. Chemical analysis of graphene oxide films after heat and chemical treatments by

X-ray photoelectron and micro-Raman spectroscopy. Carbon 2009;47:145–52.
[27] Long DH, Li W, Qiao WM, Miyawaki J, Yoon SH, Mochida I, et al. Graphitization behaviour of chemically derived graphene sheets. Nanoscale 2011;3:3652–6.
[28] Wang BG, Wang XB, Lou WJ, Hao JC. Reduced graphene oxides by microwave-assisted ionothermal treatment. New J Chem 2012;36:1684–90.
[29] Wang GX, Yang J, Park JS, Gou XL, Wang B, Liu H, et al. Facile synthesis and characterization of graphene nanosheets. J Phys Chem C 2008;112:8192–5.
[30] Paredes JI, Villar-Rodil S, Martinez-Alonso A, Tascon JMD. Graphene oxide dispersions in organic solvents. Langmuir 2008;24:10560–4.
[31] Wang Y, Zheng YQ, Huang CZ, Xia YN. Synthesis of Ag nanocubes 18–32 nm in edge length: the effects of polyol on reduction kinetics, size control, and reproducibility. J Am Chem Soc 2013;135:1941–51.
[32] Xu YX, Sheng KX, Li C, Shi GQ. Self-assembled graphene hydrogel via a one-step hydrothermal process. ACS Nano 2010;4:4324–30.
[33] Fan ZJ, Wang K, Wei T, Yan J, Song LP, Shao B. An environmentally friendly and efficient route for the reduction of graphene oxide by aluminum powder. Carbon 2010;48:1686–9.
[34] Ramesha GK, Kumara AV, Muralidhara HB, Sampath S. Graphene and graphene oxide as effective adsorbents toward anionic and cationic dyes. J Colloid Interface Sci 2011;361:270–7.
[35] Bai S, Shen XP, Zhong X, Liu Y, Zhu GX, Xu X, et al. One-pot solvothermal preparation of magnetic reduced graphene oxide–ferrite hybrids for organic dye removal. Carbon 2012;50:2337–46.
[36] Gao YJ, Ma D, Wang CL, Guan J, Bao XH. Reduced graphene oxide as a catalyst for hydrogenation of nitrobenzene at room temperature. Chem Commun 2011;47:2432–4.
[37] Sun HQ, Liu SZ, Zhou GL, Ang HM, Tade MO, Wang SB. Reduced graphene oxide for catalytic oxidation of aqueous organic pollutants. ACS Appl Mater Interfaces 2012;4:5466–71.
[38] Bai S, Shen XP, Zhu GX, Li MZ, Xi HT, Chen KM. In situ growth of Ni_xCo_{100-x} nanoparticles on reduced graphene oxide nanosheets and their magnetic and catalytic properties. ACS Appl Mater Interfaces 2012;4:2378–86.
[39] Huang JF, Vongehr S, Tang SC, Lu HM, Meng XK. Highly catalytic Pd–Ag bimetallic dendrites. J Phys Chem C 2010;114:15005–10.